Applied Soft Computing Journal 164 (2024) 111919

Contents lists available at ScienceDirect

Applied Soft Computing

journal homepage: www.elsevier.com/locate/asoc

Optimizing anomaly detection in 3D MRI scans: The role of ConvLSTM in medical image analysis

Anuradha Durairaj [a,*], E.S. Madhan [b], M. Rajkumar [c], Syed Shameem [d]

[a] Department of Computer Science and Business Systems, Panimalar Engineering College, Chennai, India
[b] School of Computer Science and Engineering, Vellore Institute of Technology, VIT University, Vellore Campus, India
[c] Department of Smart Computing, School of Computer Science Engineering and Information Systems, Vellore Institute of Technology, VIT University, Vellore Campus, India
[d] Department of Electronics and Communication Engineering, Koneru Lakshmaiah Education Foundation, Vaddeswaram, Andhra Pradesh, India

HIGHLIGHTS

- Advanced Anomaly Detection in 3D MRI.
- Deep Learning Integration.
- Crucial for ensuring data quality and consistency.
- This optimizes feature space while preserving discriminative information.

ARTICLE INFO

Keywords:
3D MRI
Long Short-Term Memory (LSTM)
Principal Component Analysis (PCA)
Anomaly detection
Convolutional Neural Network (CNN)
Machine learning
Recurrent Neural Network (RNN)
Image segmentation
Region Of Interest (ROI)
Glioblastoma

ABSTRACT

The analysis of Medical Images (MI), particularly the detection and classification of anomalies in 3D MRI (Magnetic Resonance Imaging) scans, plays a critical part in timely intervention and personalized therapy plans. In our paper, a comprehensive methodology for anomaly detection in 3D MRI scans of the brain is proposed that combines advanced Deep Learning (DL) techniques, including Convolutional Long Short-Term Memory (ConvLSTM) model, with efficient statistical feature extraction from segmented anomaly regions. The data collection phase utilizes three main datasets namely the Brain Tumor Segmentation Challenge (BRATS), the Federated Tumor Segmentation Challenge (FETS), and the Medical Segmentation Decathlon (MSD). The research begins with preprocessing steps including image resizing, intensity normalization, and alignment of anomaly region segmentation masks. The targeted anomaly regions within the samples are segmented using U-Net architecture and then follow statistical feature extraction procedure. Dimensionality reduction methods such as Principal Component Analysis (PCA) and Recursive Feature Elimination (RFE) are utilized to streamline the feature space. The ConvLSTM is then used to classify the anomalies using both convolution and recurrent layers to capture spatiotemporal patterns in MRI data. The model is fine-tuned and iterated for better classification performance using Adam optimizer. The statistical evaluation results with accuracy of 98.9 % showed that the designed ConvLSTM method is more suitable for clinical diagnosis and treatment design in detecting anomalies in 3D MRI images.

1. Introduction

Medical imaging, particularly the utilization of 3D MRI, has become indispensable in modern healthcare for diagnosing a myriad of medical conditions [1]. However, with the ever-increasing complexity and volume of MI data, the demand for advanced automated tools to assist medical professionals in image interpretation has grown exponentially [2] One critical area where these tools are indispensable is in the classification and detection of anomalies, such as cancers, in the images [3]. Brain imaging, in particular, has witnessed remarkable advancements, enabling clinicians to explore the intricate structures and functions of the central nervous system with unprecedented clarity [4]. However, the

* Corresponding author.
E-mail addresses: csbshod@panimalar.ac.in, vanu2020@gmail.com (A. Durairaj).

https://doi.org/10.1016/j.asoc.2024.111919
Received 10 November 2023; Received in revised form 13 May 2024; Accepted 22 June 2024
Available online 29 June 2024
1568-4946/© 2024 Elsevier B.V. All rights are reserved, including those for text and data mining, AI training, and similar technologies.

increasing complexity of 3D MRI data, combined with the growing demands for early and accurate diagnosis, has posed formidable challenges to MI analysis [5].

1.1. The challenge of brain imaging anomaly detection

One of the popular critical tasks in neuroimaging is the detection of abnormalities within the brain, like tumors, lesions, or other pathological conditions. These anomalies, often characterized by their subtle appearance and variability in size and location, necessitate a high level of precision and efficiency in detection [6]. Traditional methods for anomaly detection in MRI images often rely on manual interpretation by radiologists [7]. However, this method is time-consuming, dependent on inter-observer variation, and may not scale well to the increasing volume of medical data. Automated methods have emerged as a promising solution, capable of analyzing large datasets systematically and consistently [8].

1.2. DL and the promise of ConvLSTM

In recent years, DL has taken MI analysis. CNNs have demonstrated exceptional capabilities in extracting hierarchical features from 2D images, while RNNs have shown great ability to model sequential data [9]. A fusion of these two paradigms has given rise to the ConvLSTM architecture, offering a potent tool for handling the spatiotemporal complexities inherent in 3D MRI data [10]. ConvLSTM models, characterized by their ability to capture both spatial and temporal dependencies, have shown promise in a variety of applications, such as video analysis to MI processing [11]. When it comes to the detection of brain anomalies, ConvLSTMs hold the potential to harness the intricate patterns and subtle changes that may signify pathological conditions, making them an ideal candidate for automating the task of anomaly detection [12].

1.3. Statistical features and discriminative power

A crucial aspect of MI analysis, and indeed any automated anomaly detection system, lies in the choice and derivation of meaningful features [13]. The proposed research aims not only for computational efficiency but also for a high degree of discrimination. These features encapsulate essential information about the characteristics of anomalies and serve as the foundation upon which the proposed ConvLSTM-based classification model operates [14,15]. The proposed study seeks to answer a multifaceted question: How to efficiently segment anomaly regions within 3D MRI scans, derive a group of statistical features that optimally encapsulates the underlying information, as well as subsequently harness the power of ConvLSTM to classify these anomalies with unprecedented accuracy? [16] In addressing this question, we not only advance the existing MI analysis but also make strides toward more effective and timely diagnoses in clinical practice [17,18].

Although numerous 3D MRI anomaly detection approaches were available, they reflect less accuracy and high computational complexity. It is believed that using separate frameworks would help to accurately learn complicated data patterns for detection and reduce time consumed for detection. The novelty of this research lies in using a combination of approaches for each task namely, segmentation, feature extraction, dimensionality reduction, feature reduction, and classification which are significant for effective diagnosis. The state-of-art techniques generally use simple frameworks with direct application of input to the detection module. Although the process is easy to implement, faces more complications in processing tasks, resulting in high misclassification issues and high computation complexity. In our work, to boost the detection performance, and to learn the data patterns with more interpretability, separate modules are utilized for each process and finally classify the anomaly.

The contribution of anomaly detection in 3D MRI scans of the brain is as follows.

- The integration of the ConvLSTM model represents a significant contribution that enables to capture of both spatial and temporal patterns in 3D MRI data and improves anomaly detection accuracy.
- A meticulous preprocessing pipeline is established, encompassing image resizing, intensity normalization, and precise segmentation of anomaly regions. These steps are crucial for ensuring data quality and consistency.
- The research introduces a comprehensive set of statistical features, including mean, variance, skewness, kurtosis, texture features, and higher-order moments, which are efficiently extracted from segmented anomaly regions.
- PCA and RFE are employed for dimensionality reduction and feature selection. This contribution optimizes feature space while preserving discriminative information.
- The ConvLSTM architecture combines the power of CNNs and RNNs and is adapted and fine-tuned for anomaly detection in 3D MRI scans.
- The research has the potential to impact clinical practice by expediting the detection and therapy design process for individuals with glioblastoma, ultimately improving patient outcomes.

The following is the paper's overview: A review of the literature is presented in Section 2, and the general methodology for classifying anomalies is given in Section 3. The information related to experimental implementation and outcomes is provided in Section 4, finally, Section 5 concludes with recommendations for further directions.

2. Literature review

The field of MI analysis has witnessed remarkable progress over the years, driven in large part by the development of DL techniques [19]. In this comprehensive literature review, the key developments and challenges are explored in MI analysis, particularly in MRI anomaly detection. The realm of feature extraction, ConvLSTM models, and related techniques are delved to underscore the significance of the proposed study.

2.1. MI analysis

MI analysis encompasses a variety of purposes, such as diagnosing diseases, planning treatments, and monitoring. The development of DL, especially CNNs, has revolutionized the MI analysis field. CNNs have proven to be highly effective in segmentation of images, object diagnosis, as well as classification. For example, the U-Net structure has become a cornerstone in MI segmentation, offering existing results in several applications [20].

2.2. MRI anomaly detection

MRI anomaly detection has emerged as a critical area of study, particularly in fields such as neurology and oncology [21]. MRI is a cornerstone in neuroimaging, providing detailed information about the brain's structure and function. In the context of anomaly detection, MRI has been instrumental in identifying various pathologies, including tumors, lesions, and neurodegenerative disorders [22]. Traditional approaches to MRI anomaly detection often involve rule-based systems and manual intervention, which are time-consuming and subjective.

Recent years have seen a surge in automated MRI anomaly detection methods. Notably, DL methods have been used in this domain, offering the potential for faster and more consistent diagnoses. Conventional CNNs have been employed for binary classification tasks, distinguishing between normal and abnormal scans [23]. However, these models may struggle with the nuanced classification of different anomaly subtypes, necessitating more sophisticated approaches.

Table 1
Outline of literary works.

Authors	Designed system	Dataset	Objectives	Advantage	Limitation
Raza et al. [32]	DeepTumorNet	CE-MRI	To develop DeepTumorNet, a hybrid DL method, for accurate brain tumor classification	According to MRI images, this model proved to be better for BT classification	High time complexity
Tazin et al. [33]	Transfer Learning with MobileNetV2	Brain tumor	To enhance brain tumor identification from X-ray images using CNNs with transfer learning techniques	This method was the most successful way to diagnose brain tumors	Poor generalization
Rao et al. [34]	Kernel-based Support Vector Machine	BRATS 2018, 2019 and 2020	To develop an efficient segmentation and classification method for brain tumors using ML models	Higher diagnostics accuracy provides early and accurate diagnosis, helping to save lives	Complex and computationally expensive
Garg et al. [35]	Hybrid KNN-RF-DT	Benign and Malignant classification	To develop a hybrid ensemble method for brain tumor classification	This method offers high accuracy at the cost of increasing the complexity of training time	Limited ability to deal with complex patterns and contrasts present in MRI images
Chintalapudi et al. [36]	Gradient boosting and XG boosting	BRATS	To utilize Gradient as well as XG boosting algorithms for accurate brain tumor classification	This method obtained a better performance in brain tumor classification	Demand high computational resources

2.3. Feature extraction in MI

The most significant aspect of MI analysis is feature extraction. The selection and extraction of relevant features greatly impact the performance of subsequent classification models. In MRI anomaly detection, different groups of features exploded, including Intensity-based features (IBF), texture features (TF), and shape-based features (SBF) [24,25].

IBF encompasses statistical measures of voxel intensities within regions of interest (ROIs). Common features include mean intensity, variance, skewness, and kurtosis. These features capture the distributional characteristics of intensity values and have been used successfully in anomaly detection tasks [26].

Texture features extend the analysis beyond simple intensity statistics. Methods including the Gray-Level Co-occurrence Matrix (GLCM), Laws' texture energy measures, as well as Haralick textures have been applied to capture spatial patterns within MRI images [27]. These features provide valuable insights into the textural properties of anomalies.

Shape-based features focus on the geometrical characteristics of segmented regions. These features encompass measures like volume, surface area, compactness, and eccentricity, providing information about the shape and morphology of anomalies. They have been instrumental in distinguishing between different anomaly subtypes [28].

Despite the progress in feature extraction techniques, there exists a gap in research that effectively combines the power of statistical, texture, and shape features while ensuring computational efficiency. The objective of proposed research is to overcome this gap by deriving a comprehensive yet discriminative set of statistical features that enhance anomaly classification in 3D MRI scans.

2.4. ConvLSTM models

ConvLSTM models represent a fusion of CNNs and RNNs, offering a unique capacity to capture both spatial and temporal dependencies within sequential data. These models have found success in video analysis, action recognition, and various spatiotemporal tasks.

In the realm of MI analysis, ConvLSTMs have been demonstrated in tasks that involve 4D (3D spatial + temporal) data. For instance, they have been used in cardiac image analysis to segment and monitor the heart over time [29]. However, their potential in 3D MRI anomaly detection remains relatively underexplored.

2.5. Relevant studies and techniques

ConvLSTMs are used in a variety of ways in MI analysis. Various studies have shown their versatility and effectiveness. For instance, ConvLSTMs are used to detect and classify lung nodules on computed tomography (CT) scans, achieving superior performance based on accuracy and false-positive (FP) rates. This highlights the potential of ConvLSTMs in detecting subtle abnormalities in MI [30].

Additionally, recent research by demonstrated the utility of RNN, including ConvLSTMs, in the segmentation. The model's ability to identify temporal dependencies within the information proved valuable for precise tumor delineation. This study underscores the relevance of recurrent architectures, such as ConvLSTMs, in handling sequential and volumetric medical data [31]. Raza et al. [32] developed the DeepTumorNet (DTNet) model for classifying brain tumors. The DTNet was developed by adding 15 additional layers in GoogLeNet architecture and removing 5 layers. The expensiveness of the model was increased using leaky ReLU. Finally, the model was evaluated and better accuracy was achieved. Tazin et al. [33] presented a CNN for brain tumor detection. Tumor images were extracted from a publicly obtainable tumor dataset. In a preprocessing step, the image was resized, then the collection of images in the array was processed and finally, coding was performed. The experiment was performed using Python and Google Colab and attained a high boosting accuracy.

Rao et al. [34] utilized a Support Vector Machine (SVM) for the classification of tumors. The Blur was removed and the quality was enhanced using a Normalized median filter. After preprocessing, segmentation was performed using the binomial thresholding method. The fusion of gray level and fusion GLCM was utilized for extracted features and Harris Hawks optimization for feature selection. Finally, the tumor was classified with high accuracy. Garg et al. [35] employed the K Nearest Neighbor-Random Forest-Decision Tree (KNN-RF-DT) ensemble method to estimate tumor area and classify tumor. In the first step, Otsu's Threshold method was applied for segmentation. Next, the combination of principle analysis components, stationary wavelet transform and GLCM were employed for feature extraction. According to the major voting method, the classification was performed and superior accuracy was achieved. Chintalapudi et al. [36] utilized the Gradient Boosting Machine method for classifying tumors. The data was collected from BraTS 2015 dataset as well as BT features were identified using the correlation matrix. The classification was performed using GBM and high accuracy was attained. Table 1 outlines the summary of literary works.

2.6. Gaps in existing research and justification

While these studies demonstrate the promise of ConvLSTM models in various MI analysis tasks, there are notable gaps in the existing literature that warrant further investigation.

- *Efficient Feature Extraction*: Many studies employ complex neural architectures for feature extraction, often leading to high computational costs and increased model complexity. There is a need for research focused on deriving efficient yet informative features from medical imaging data, especially in the context of anomaly detection.

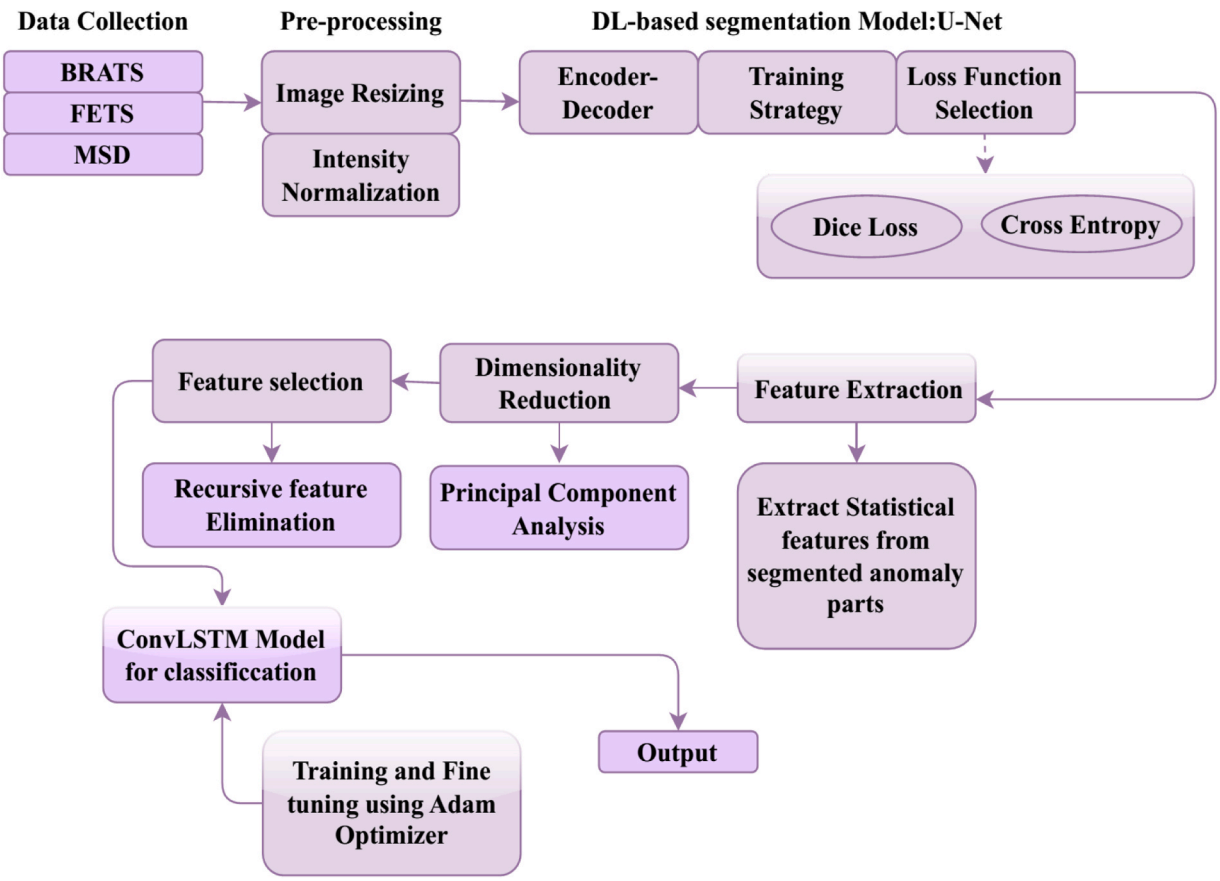

Fig. 1. Outline of proposed methodology.

- *Combining Feature Extraction with ConvLSTM*: Existing research often focuses on either feature extraction or ConvLSTM-based classification separately. A comprehensive approach that integrates efficient feature extraction with ConvLSTM-based classification for anomaly detection is an underexplored area.
- *Generalization and Benchmarking*: While ConvLSTMs have shown promise in specific MI analysis tasks, their generalizability across different datasets and clinical scenarios remains uncertain. There is a need for benchmarking studies that assess the performance of ConvLSTM-based approaches across diverse medical imaging datasets.

The proposed research addresses these gaps in the existing literature by proposing an integrated approach. The model aims to efficiently extract informative statistical features from segmented anomaly parts of 3D MRI scans and employ ConvLSTM models for precise anomaly classification. By combining these components, the proposed study seeks to provide a holistic solution for automated anomaly diagnosis in MI.

Furthermore, the proposed approach is evaluated on datasets, including the BRATS, FETS, and MSD datasets. This evaluation will not only demonstrate the suggested method's efficacy and assess its generalizability and possibility for practical clinical applications.

In summary, the integration of efficient feature extraction, ConvLSTM-based classification, and comprehensive evaluation of benchmark datasets makes the proposed study relevant, impactful, and poised to advance the existing MI analysis, especially in realm of MRI anomaly detection.

3. Methodology

Fig. 1 presents an outline of suggested methodology. First, we use data acquisition for 3D MRI scan collection and organization. Next, the collected 3D MRI scans are resized and normalized. Further, a U-Net architecture is utilized to segment anomaly regions as well as extract statistical features such as texture features, histogram-based features, mean, kurtosis, etc. We utilize PCA and RFE methods to minimize dimensionality and to select the most discriminative features. The ConvLSTM is made up of 2 convolution layers, a pooling layer, 2 LSTM layers, a flattened layer, and 2 fully connected layers. It has a sigmoid activation function used for anomaly detection and classification. Finally, fine-tuning and iterations are performed to improve classification performance.

3.1. Data collection and preprocessing

In this part, a comprehensive overview of database utilized in the proposed research, the preprocessing steps applied, and the rationale behind these processes are provided.

3.1.1. Data collection

For the proposed research, three key datasets: the BRATS, FETS, and MSD are leveraged. These datasets offer diverse MRI scans, serving as crucial benchmarks for anomaly detection in brain imaging.

3.1.2. Data preprocessing

Effective data preprocessing is an important part of ensuring the quality and consistency of proposed input data. The MRI volumes are prepared to facilitate uniformity and robustness in subsequent DL-based segmentation and feature extraction processes. The following preprocessing steps are integral to the proposed methodology.

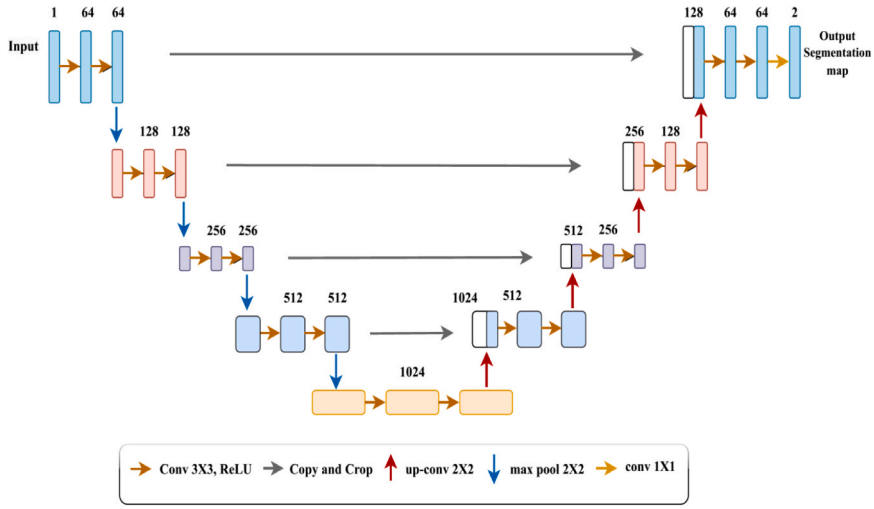

Fig. 2. Architecture of U-Net model.

3.1.3. Image resizing

In this step, resize all MRI volumes to a standardized resolution to ensure uniform input sizes for the DL models. This operation is crucial for seamless model training and feature extraction across the dataset. The resizing process is carried out using the following formula:

$$I_r = R(I_o, t_s) \tag{1}$$

where I_r represents the resized MRI image, I_o denotes the original MRI image and t_s specifies the desired standardized resolution.

3.1.4. Intensity normalization

Intensity normalization techniques are applied to normalize the intensity values for various MRI modalities, ensuring that the proposed models are robust to variations in image acquisition settings. The Z-score standardization technique is employed and is expressed as:

$$Z_{score} = \frac{I - \mu}{\sigma} \tag{2}$$

where Idenotes the Original Intensity value in original MRI image, μ denotes the mean intensity value across the entire MRI volume, and σrepresents the standard deviation of intensity values in the MRI volume. This normalization process ensures that the mean intensity becomes zero, and the standard deviation becomes one, effectively standardizing the intensity distribution across all MRI scans.

3.1.5. Anomaly region segmentation masks

Ground-truth segmentation masks, meticulously annotated by radiologists, serve as the foundation for extracting anomaly regions. These masks delineate the regions of interest, precisely identifying anomaly locations. To ensure alignment between these masks and resized images, a spatial transformation function is employed, which is applied as follows:

$$T_M = S(O_M, \phi) \tag{3}$$

where $T_M$represents transformed mask, O_M represents original mask or manually annotated segmentation mask, S denotes spatial transformation, and ϕ represents transformation parameters. Transformation Parameters encompass translation, rotation, and scaling parameters necessary to match the mask to the resized MRI image. The spatial transformation process guarantees that the segmentation mask precisely corresponds to the resized MRI data, ensuring accurate extraction of anomaly regions.

3.2. DL-based segmentation model: U-Net for anomaly region segmentation

In this section, a highly effective segmentation of U-Net model of anomaly regions within MRI volumes is detailed.

3.2.1. U-Net architecture overview

The preprocessed samples from preprocessing procedure are taken as input. For segmenting anomaly regions within the MRI scans, the existing DL model, the U-Net architecture is used. The U-Net (shown in Fig. 2) has a proven track record for exceptional performance in semantic segmentation applications and is well-suited to segmenting structures with complex shapes, such as tumors.

The U-Net structure comprises the decoder and encoder. The encoder captures hierarchical features, while the decoder generates segmentation masks at multiple scales. The U-Net architecture is adapted to handle multi-modal MRI data by incorporating parallel pathways for each MRI modality and merging their feature representations before segmentation.

3.2.2. Training strategy

To make sure the model is efficient and robust, a meticulous training strategy is employed. The database is categorized into training, validation, and testing subsets, adhering to the following formulas for partitioning:

$$\text{Training Set } D_{train} = \frac{100}{N} \times T_p \tag{4}$$

$$\text{Validation Set } D_{val} = \frac{100}{N} \times V_p \tag{5}$$

$$\text{Testing Set } D_{test} = N - D_{train} - D_{val} \tag{6}$$

here N represents the overall sample count in a dataset, $T_p$denotes training percentage i.e., the data proportion allocated to the training set, $V_p$denotes validation percentage i.e., data proportion allocated to validation set.

The model training is commenced using a subset of the BRATS dataset, leveraging the D_{train} samples. Subsequently, to enhance the model's generalization across different data sources, the U-Net architecture is fine-tuned using samples from the FETS and MSD datasets.

3.2.3. Loss function

Selecting an appropriate loss function is crucial for training U-Net model to perform accurate segmentation. Two loss functions employed

in MI segmentation: Dice loss (DC) and cross-entropy loss (CEL). The experiment is conducted on different loss functions and selects the one that optimizes segmentation performance.

DC: DC measures the overlap among the ground-truth mask and the anticipated segmentation; it is also referred to as the Sorensen-Dice coefficient. It is stated as follows:

$$D_L = 1 - \frac{2 \times (P \cap G)}{(P \cup G) + \in} \tag{7}$$

here Pindicates U-Net model anticipated by the segmented mask, G denotes manually annotated ground-truth segmented mask, $\cap$indicates intersection of 2 masks, $\cup$signifies the union of 2 masks, and $\in$ represents a small constant added for numerical stability. The Dice loss incentivizes the model to generate segmentations that closely resemble the ground truth, rewarding high overlap between the two masks.

Cross-Entropy Loss: The dissimilarity among the binary ground-truth mask and anticipated segmented probability map is measured by CEL, that is frequently used in image segmentation. It is computed as follows:

$$CE_L = -\sum_{i,j} (G(i,j) \cdot \log(P(i,j))) \tag{8}$$

where $G(i,j)$ indicates ground truth mask with binary rate (0 or 1), $P(i,j)$represents predicted probability belonging to the anomaly region. The cross-entropy loss penalizes the model for deviations between its predictions and the ground-truth binary mask, effectively guiding it to produce accurate segmentation.

3.3. Statistical feature extraction

After obtaining the U-Net segmentation masks for the anomaly regions, the statistics are extracted from the segmented regions. This step is essential for characterizing the anomalies in a manner conducive to subsequent classification.

3.3.1. Mean

Calculating the mean intensity of the voxel values within segmented anomaly parts provides a measure of central tendency.

$$\mu = \frac{1}{N} \sum_{i=1}^{N} I_i \tag{9}$$

whereμ represents the mean intensity within the segmented anomaly region, $N$is the overall voxel count in segmented region, and I_i denotes intensity value of voxel iCalculating the mean intensity provides insights into the average intensity of the anomaly region, serving as a fundamental descriptor of its overall brightness.

3.3.2. Variance

Determining the variance of voxel intensities to assess the spread or dispersion of intensity values within the anomaly.

$$\sigma^2 = \frac{1}{N} \sum_{i=1}^{N} (I_i - \mu)^2 \tag{10}$$

Where σ^2 represents the variance of intensity values within the segmented anomaly region, N is the overall voxel count, I_i denotes intensity rate of voxel i, and μ represents the mean intensity. Variance measures the spread or dispersion of intensity values within the anomaly region, providing insights into the distribution's variability.

3.3.3. Skewness

Skewness quantifies the asymmetry of the intensity distribution, indicating whether the distribution is skewed towards higher or lower values.

$$\gamma_1 = \frac{\frac{1}{N}\sum_{i=1}^{N} (I_i - \mu)^3}{\sigma^3} \tag{11}$$

Where γ_1 represents the skewness of the intensity distribution within the segmented anomaly region, N is the overall voxels count, I_i denotes intensity rate of voxel i, μ represents the mean intensity and σ^3 is the cube of the standard deviation.

3.3.4. Kurtosis

Kurtosis captures whether the intensity distribution is peaky or flat, indicating whether it is more or less concentrated around the mean.

$$\gamma_2 = \frac{\frac{1}{N}\sum_{i=1}^{N} (I_i - \mu)^4}{\sigma^4} \tag{12}$$

where γ_2 represents the kurtosis of the intensity distribution within the segmented anomaly region, Nrepresents the overall voxel count, I_i indicates the intensity value of voxel i, μ is the mean intensity, and σ^4 is the fourth power of the standard deviation.

3.3.5. Histogram-based features

The histograms of voxel intensities are conducted within the anomaly region and derive features such as entropy, energy, mode, and percentiles. These features offer a comprehensive view of the intensity distribution, including its randomness, dominant values, and spread.

3.3.6. Texture features

Utilizing texture analysis methods, including GLCM and Haralick textures, on the voxel intensities captures textural patterns within the anomalies. These features encompass properties like contrast, homogeneity, and texture energy.

3.3.7. Higher-order moments

Beyond kurtosis, skewness and higher-order moments, including quartile skewness and excess kurtosis are implemented for a more detailed characterization of the intensity distribution. These moments capture nuances in the distribution shape.

3.3.8. Spatial statistical features

The statistical measures are extended to include spatial statistics, considering the relationships between neighboring voxels within the anomaly region. Features like spatial correlation and co-occurrence matrices enhance the understanding of spatial patterns, offering insights into the arrangement of intensity values.

3.3.9. Shape-related features

From the segmented anomaly region, shape-related statistics, including volume, surface area, compactness, and eccentricity are extracted. These features provide geometric information about the shape and structure of the anomalies.

3.4. Dimensionality reduction and feature selection

The high dimensionality of the extracted statistical features introduces redundancy and increases computational complexity. Therefore, PCA and RFE are applied to address these challenges.

3.4.1. PCA

The high dimension of extracted statistical features leads to computational complexity and potential overfitting. The PCA is applied to minimize dimensionality while retaining the most informative features. PCA finds orthogonal components (principal components) that gather for the maximum variability in the information, allowing us to represent the data in a reduced-dimensional space. PCA is achieved through the eigen decomposition of the covariance matrix of the original feature space. The eigenvectors of this matrix represent the principal

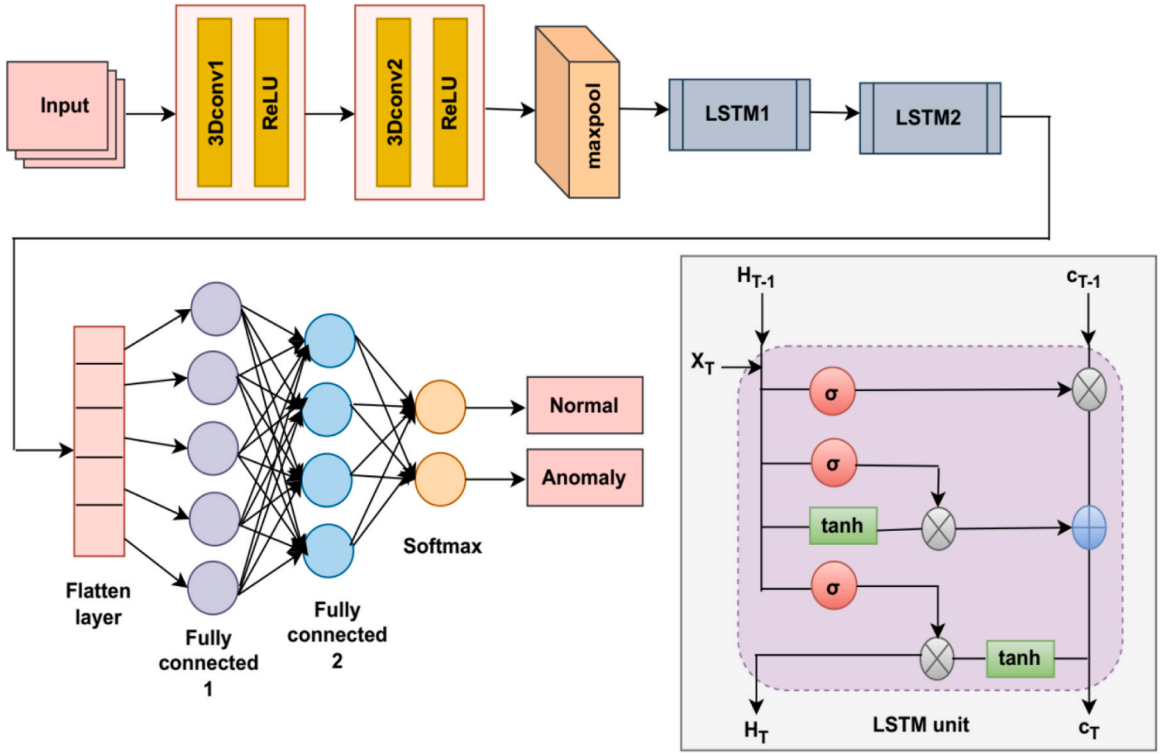

Fig. 3. Overview of ConvLSTM.

components.

$$\sum = \frac{1}{N}\sum_{i=1}^{N}(X_i - \overline{X})(X_i - \overline{X})^T \tag{13}$$

Where $\sum$is the covariance matrix, $N$is the sample count, $X_i$denotes the i^{th}information point, and $\overline{X}$represents the mean of the data points. PCA identifies the principal components PC_1,PC_2,…PC_kalong with their corresponding eigenvalue λ_1,λ_2…λ_k. These components capture the most important directions in the data.

3.4.1.1. Component selection. To manage dimensionality while retaining critical information, a subset of principal components is selected that retain a predefined percentage of the total variance. This selection ensures a balance between dimensionality reduction and information retention.

$$\text{Variance explained} = \frac{\sum_{i=1}^{k}\lambda_i}{\sum_{i=1}^{N}\lambda_i} \tag{14}$$

Where λ represents the eigenvalue associated with the i^{th}principal component and $k$indicates the amount of principal components selected.

3.4.2. Recursive feature elimination (RFE)

In addition to PCA, RFE is used to further enhance feature selection. RFE is a powerful method that iteratively eliminates low-significant features, ranking them based on their contribution to classification performance.

3.4.2.1. Feature ranking. RFE assigns importance scores to each feature according to their effect on model's effectiveness. The ranking helps identify and retain the most discriminative features for classification.

$$F = P(A) \tag{15}$$

Where F represents feature importance score, P represents performance metric, and Arepresents accuracy. During each iteration, RFE eliminates the feature with the lowest importance score, progressively reducing feature space while keeping the major valuable features.

By using PCA for dimensionality reduction and RFE for feature selection, the feature space is streamlined, ensuring that the proposed ConvLSTM model operates efficiently while maintaining discriminative power for anomaly classification.

3.5. ConvLSTM model for classification

Following the feature selection process, the proposed ConvLSTM method, meticulously structured for anomaly detection and classification, takes center stage. It plays a pivotal role in capturing the spatio-temporal patterns present in 3D MRI data. A ConvLSTM model is designed with a suitable structure that leverages both convolutional and recurrent layers for effective anomaly classification. The ConvLSTM architecture integrates the advantages of CNNs and RNNs to effectively capture temporal and spatial patterns within the 3D MRI data. The overview of ConvLSTM is given in Fig. 3. The input layer comprises selected statistical features. The middle layer comprises convolutional, Maxpooling, LSTM, flattening, and fully connected layers. The output attempts to detect and classify anomalies.

3.5.1. 3D convolutional layers

To extract meaningful spatial features from segmented anomaly regions, a stack of convolutional layers is employed. These layers perform 3D convolutions on the input statistical features, allowing the model to recognize local patterns within the data. The depth and width of the convolutional layers are optimized to balance feature extraction and model complexity.

3.5.2. ConvLSTM layers

The core of the proposed architecture consists of ConvLSTM layers. ConvLSTM units are integrated to model the temporal dependencies across slices of the 3D MRI data effectively. These units extend the conventional LSTM architecture by incorporating convolutional operations within the gates, making them well-suited for spatiotemporal data.

The ConvLSTM layers help the proposed model capture the dynamic behavior of anomalies within the volumetric data. The spatial correlation problem in LSTM is solved using the ConvLSTM. The ConvLSTM equation is determined as:

$$I_T = \sigma(w_{XI} * x_T + w_{HI} * h_{T-1} + w_{CI} \circ c_{T-1} + b_I) \tag{16}$$

$$F_T = \sigma(w_{XF} * x_T + w_{HF} * h_{T-1} + w_{CF} \circ c_{T-1} + b_F) \tag{17}$$

$$c_T = F_T \circ c_{T-1} + I_T \circ \tanh(w_{XC} * x_T + w_{HC} * h_{T-1} + b_C) \tag{18}$$

$$O_T = \sigma(w_{XO} * x_T + w_{HO} * h_{T-1} + w_{CO} \circ c_{T-1} + b_O) \tag{19}$$

$$h_T = O_T \circ \tanh(c_T) \tag{20}$$

where F_T, I_T, O_T, and c_T denotes the forget gate, input gate output gate, and memory cell respectively.

3.5.3. Pooling and flattening

To reduce spatial dimensions and extract the most salient features, the pooling layers are employed within the ConvLSTM stack. This operation is essential for hierarchical feature extraction. Subsequently, the output is flattened to prepare it for classification.

3.5.4. Fully connected layers

Following the ConvLSTM stack, to introduce fully connected layers. The layers provide the method with the capacity to learn high-level representations of the anomaly regions. The neuron count and depth of layers are fine-tuned to optimize classification performance.

3.5.5. Output layer

The layer of output is composed of the activation function of sigmoid that transforms the method's output into class probabilities. In the binary classification task (normal vs. anomaly), the model outputs the probability of an anomaly presence within the segmented region.

The proposed ConvLSTM model, with its precise architectural structure, efficiently processes the selected statistical features. It commences with convolutional layers to capture spatial patterns, succeeded by LSTM layers to model temporal dependencies. Fully connected layers facilitate the fusion of spatial and temporal features, ultimately leading to the final classification results in the output layer. Typically, for MI analysis like anomaly detection in 3D MRI scans, output of ConvLSTM model is probability or a set of probabilities associated with each class or category. For performing binary classification (e.g., anomaly or non-anomaly), the ConvLSTM model's output is a single probabilistic value between zero and one. This probability represents likelihood that the input 3D MRI scan contains an anomaly. A threshold (usually 0.5) is applied to this probability to make a binary decision: anomaly or non-anomaly. Example Output: Probability of Anomaly (e.g., 0.75)

4. Experimental results

This part describes the experimental design for the suggested method. To classify segmented anomalies, three datasets are utilized. The database is divided into train, test, and validation. Typically around 70 % of data is utilized to train the method. The MRI scans of patients with glioblastoma are included in this dataset, along with the manually annotated ground-truth segment labels of the corresponding cancer subregions.

Pre-processing: The 3D MRI images collected from datasets undergo initial processing such as resizing and normalization which enables the system easier to process data without any data variation complexities.

Data Feeding: The selected statistical features, previously extracted from MRI scans, serve as the model's input. These features are pre-processed to match the model's input specifications.

Loss Function: During training, the model minimizes a specific loss function tailored to the classification task. For binary-class *classification*, binary cross-entropy is employed.

Table 2
Hyperparameters and value.

Hyperparameter	Search range	Value
Learning Rate, LR	[0.001, 0.1]	0.001
Batch Size, BS	[32, 128]	32
Number of Epochs	[50, 100]	50
No. of convolutional Layers	[2, 3]	2
Number of filters in 1st and 2nd layer	[24, 32, 64, 128]	32 and 64
Spatial size of CNN filters	[2 × 2, 3 × 3, 5 × 5, 7 × 7]	3 × 3
LSTM Layers	[64, 128]	64 units
Dropout Rate	[0.25, 0.5]	0.3
No. of fully connected layers	[1, 2, 3]	2
Total units in 1st and 2nd fully connected layers	[24, 32, 64, 128]	128 units, 64 units
Activation Function	[tanH, sigmoid]	Sigmoid
Threshold (Binary Class.)	[0.5, 0.75]	0.5
PCA Components	[50,100]	100
RFE Features	[50,100]	50

Optimization: To used an optimization algorithm, such as Adam optimizer, and update the model's parameters iteratively and reduce loss function. The hyperparameters, namely learning rate (η), are *optimized* through experimentation and validation.

Batch Processing: To enhance training stability, data is processed in batches. This allows the model to update its parameters incrementally, with the batch size (B) being another hyperparameter fine-tuned for optimal performance.

Epochs: Training spans multiple epochs (E), with the entire training dataset being processed in each epoch. The number of epochs is selected carefully to achieve convergence without overfitting.

To monitor the model's performance during training and prevent overfitting, a smaller segment is reserved, usually 15 % of the data, as the validation dataset. This set also includes 3D MRI scans and their respective ground-truth labels. Following each training epoch, the model is evaluated on the validation database utilizing a set of measures computed to monitor the model's progress as well as detect signs of overfitting.

The remaining 15 % of the data is designated as a testing dataset. This dataset is unseen during training and is vital for assessing the method's generalization capability. Similar to the train and validation datasets, it contains ground-truth labels and 3D MRI scans. Once training is complete, the final evaluation takes place on the testing dataset. This dataset represents unseen data, enabling us to gauge the model's real-world performance accurately. A comprehensive evaluation metric is reported to quantify the model's ability to accurately classify anomalies within 3D MRI scans.

Cross-validation methods, like k-fold cross-validation, are used to strengthen the model. This entails the database dividing into multiple subsets, training and validating on various combinations, as well as aggregating the results to provide a more reliable estimate of performance.

Fine-tuning and iteration are performed to improve the accuracy of anomaly classification and diagnosis.

Throughout these sections, sufficient detail, including hyperparameter settings, specific metrics, and qualitative observations is provided. This enables readers to understand the methodology's effectiveness and reproducibility.

4.1. Experimental setup

The implementation of an experiment is performed using Python 3.10.11 with an operating system 64-bit, Intel Core i3, as well as 8.00 GB RAM.

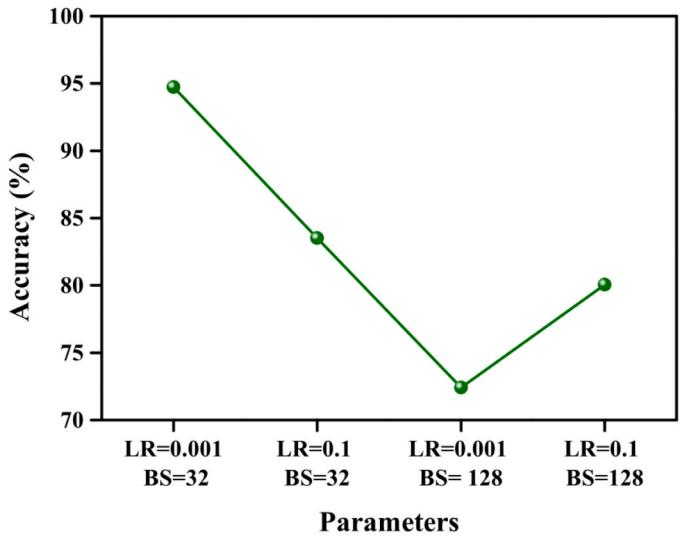

Fig. 4. Parameter sensitivity analysis.

4.2. Hyperparameter configuration

The hyperparameters used for anomaly classification selected using Adam optimizer are illustrated in Table 2. Beside, pre-defining the parameter values, the proposed ConvLSTM parameters (described in Table 2) are fixed by iterative experiment using Adam. It selects the suitable combination of parameter values for the model with high accuracy. Fig. 4 displays the parameter sensitivity analysis in terms of accuracy using two learnable factors such as learning rate and batch size.

4.3. Dataset description

For the proposed research, three key datasets: BRATS, FETS, and MSD datasets are used. These datasets offer diverse MRI scans, serving as crucial benchmarks for anomaly detection in brain imaging.

4.3.1. BRATS dataset

The BRATS dataset includes medically obtained glioblastoma of MRI scans individuals [37–39]. The dataset consists of 1675 total MRIs, with 1173 training, 167 validation, and 335 testing MRIs. The dataset includes total MRI for all conditions 418 T1-weighted, 419 T2-weighted, 419 contrast-enhanced T1-weighted (CETW), and 419 FLAIR sequences. Notably, the dataset provides hand annotations by radiotherapists, serving as ground-truth segmented labels of cancer sub-levels. The BRATS dataset is used for train, validation, and testing of the ConvLSTM-based anomaly detection model.

4.3.2. FETS dataset

The FETS 2021 dataset, comprising 1251 total scans, is the first Fed-DL dataset of MI. It was gathered from various sites using various clinical protocols. FETS is made up of a collection of glioblastoma scans from additional independent institutions as well as a subset of glioblastoma scans from a Brain cancer Segmentation that includes institutional

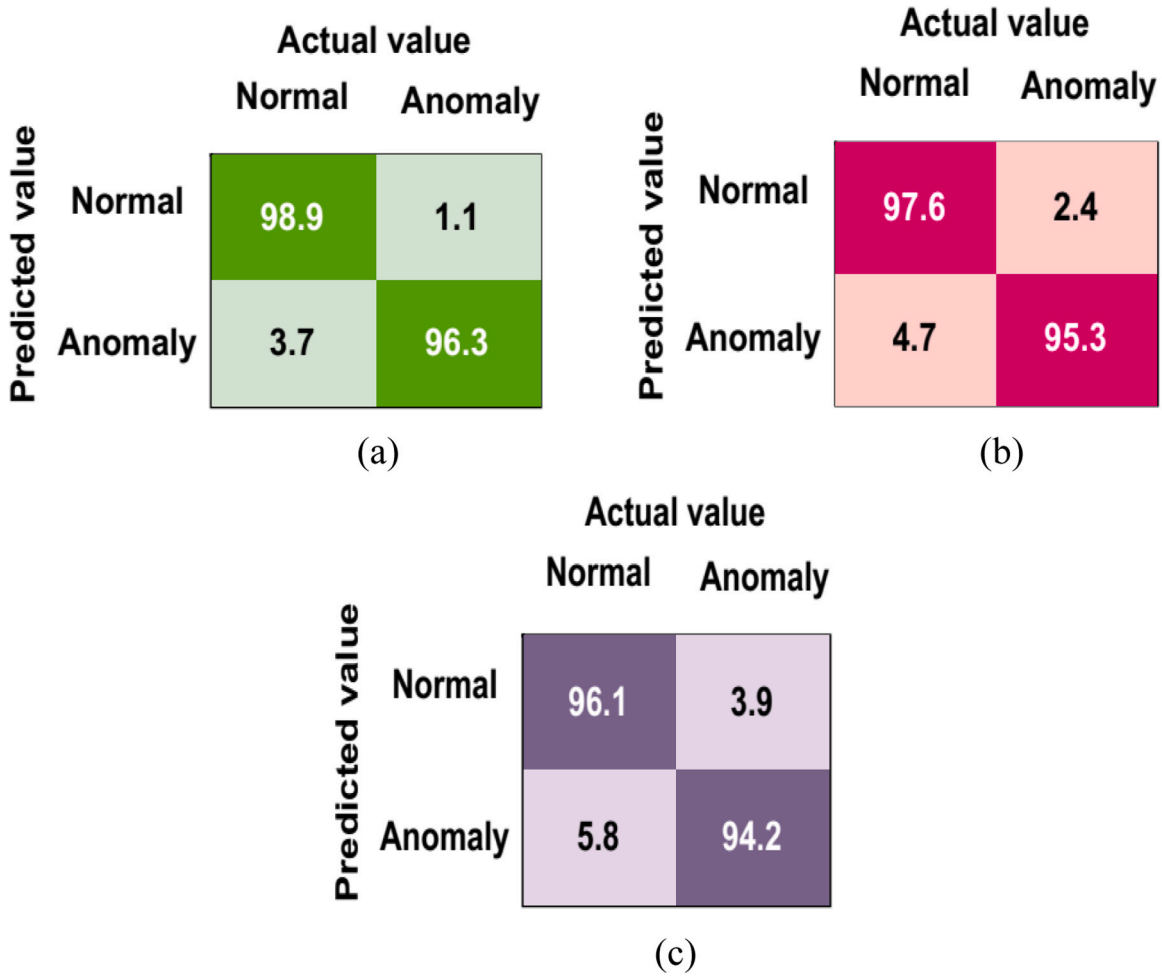

Fig. 5. Confusion matrix (a) BraTS 2019 dataset (b) FETS dataset (c) MSD dataset.

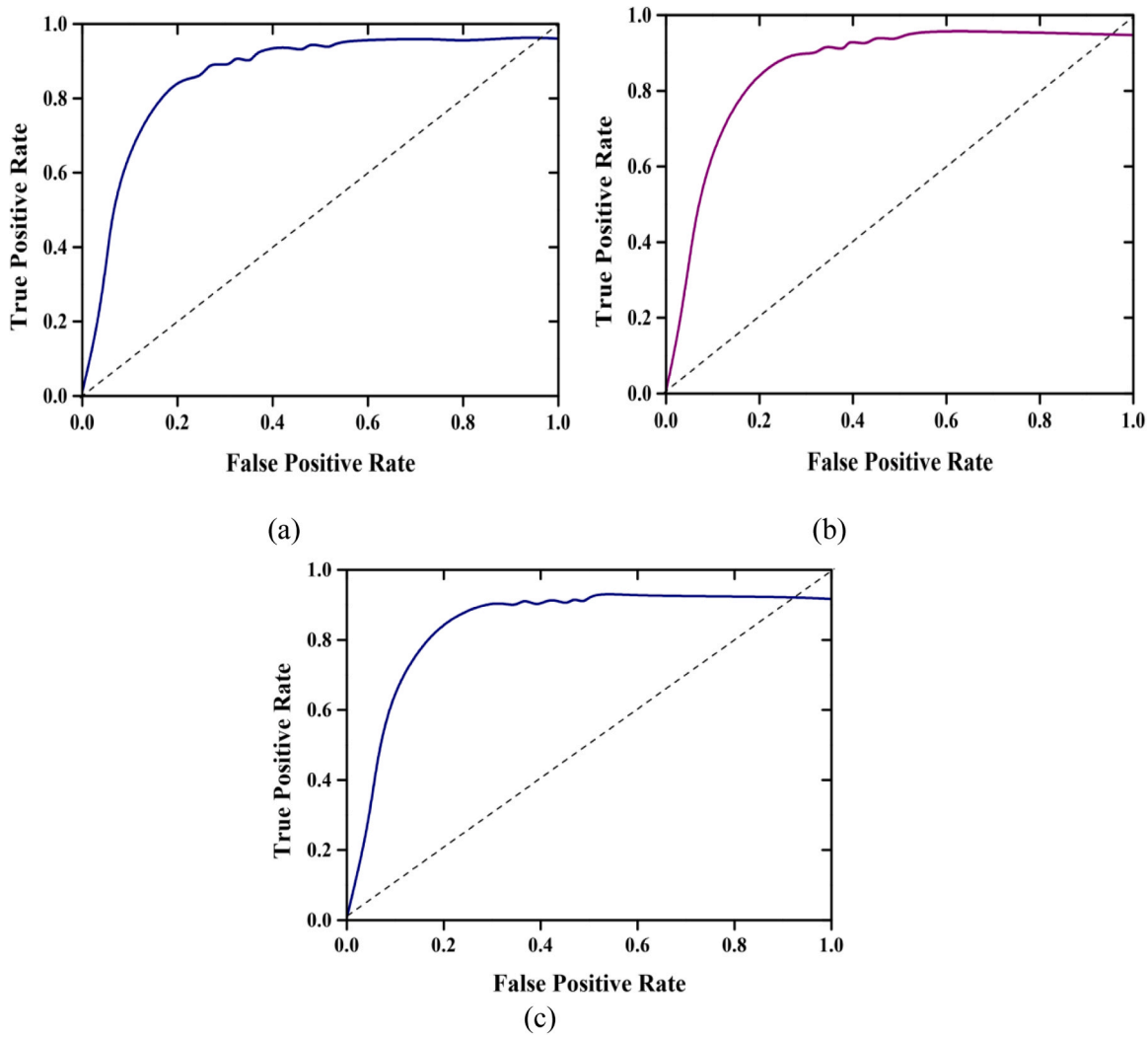

Fig. 6. AUC (a) BraTS 2019 dataset (b) FETS dataset (c) MSD dataset.

information [40]. T1-weighted, T2-weighted, CETW, and FLAIR are the four series that make up every FETS scan.

4.3.3. MSD dataset

The MSD dataset is group of MI datasets commonly used for segmentation algorithms testing and benchmarking. The dataset includes images from several imaging conditions like MRI, CT, and ultrasound, covering a range of anatomical structures and diseases [41,42]. The dataset is divided into ten challenges. Each challenge focuses on a particular segmentation challenge associated with various organs or tissues in the medical imaging domain. Researchers use MSD datasets for segmentation algorithm development and benchmarking for medical applications.

4.4. Performance evaluation metrics

Accuracy (A): Accuracy defines the difference between the accuracy of the result to the overall detection. The equation is given as:

$$A = \frac{a_{TP} + a_{TN}}{a_{TP} + a_{TN} + a_{FP} + a_{FN}} \tag{21}$$

where a_{TP}denotes true positive (TP), a_{TN} denotes true negative (TN), a_{FP}denotes false positive (FP), and a_{FN}denotes false negative (FN).

Precision (P): The difference between TP and the total of TP and FP results are obtained using precision. The equation is stated as:

$$P = \frac{a_{TP}}{a_{TP} + a_{FP}} \tag{22}$$

Sensitivity (S): The ratio of relevant and retrieved results to the relevant result is sensitivity. It is also known as recall and the equation is presented as:

$$S = \frac{a_{TP}}{a_{TP} + a_{FN}} \tag{23}$$

Specificity (SP): The difference between the TP result to the total of FP and TN is specificity. The equation is provided below:

$$SP = \frac{a_{TN}}{a_{TN} + a_{FP}} \tag{24}$$

F1 score (F1): The balance between precision and recall is measured using the F1 score and the equation is provided as:

$$F_1 = 2 * \frac{P * S}{P + S} \tag{25}$$

The area under curve (AUC): AUC calculates the method performance on unbalanced data and the range is between 0 and 1.

4.5. Performance analysis

The performance evaluation of the BraTS 2019 dataset, FETS dataset, and MSD dataset are provided in this section.

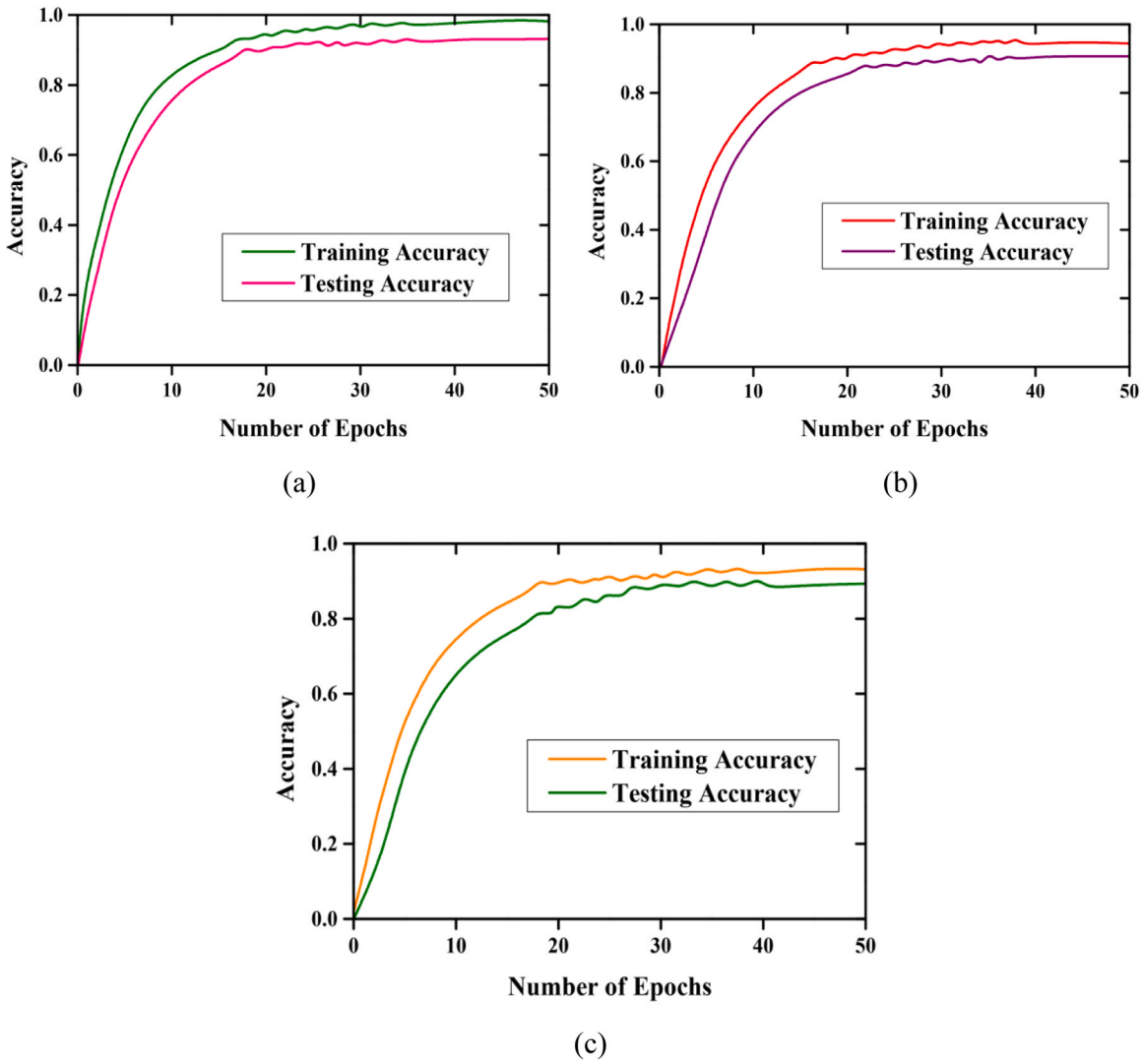

Fig. 7. Training and testing accuracy (a) BraTS 2019 dataset (b) FETS dataset (c) MSD dataset.

Fig. 5(a–c) shows the confusion matrix for the BraTS 2019, FETS, and MSD datasets, and the classification performance for normal and anomaly. In the BraTS 2019 dataset, 98.9 % of instances were correctly classified as normal, while 1.1 % were misclassified as anomalies. Conversely, 96.3 % of anomalies were accurately identified, with 3.7 % misclassified as normal. Similarly, in the FETS dataset, 97.6 % of instances were correctly classified as normal, while 2.4 % were misclassified as anomalies. Meanwhile, 95.3 % of anomalies were accurately identified, with 4.7 % misclassified as normal. In the MSD dataset, 96.1 % of instances were correctly classified as normal, with 3.9 % misclassified as anomalies. Conversely, 94.2 % of anomalies were accurately identified, with 5.8 % misclassified as normal. These results suggest a high level of accuracy for normal instances, while anomalies were slightly misclassified across datasets.

Fig. 6(a–c) depicts the AUC-ROC for BraTS 2019, FETS, and MSD datasets. The total quantity of performance over all possible classification thresholds is offered using the AUC-ROC. The ROC ranks between 0 and 1. The BraTS 2019, FETS, and MSD datasets achieved AUC-ROC values of 0.98, 0.97 and 0.96 correspondingly. It indicates its effectiveness in classifying events in the dataset. These results show the efficacy of our classification methods used across all datasets.

Fig. 7(a–c) shows training and testing accuracy plotted from 0 to 50 epochs for the testing and training dataset. The results demonstrate promising performance across all datasets. BraTS achieved training and testing accuracy of 0.97 and 0.94, respectively. FETS accuracy is 0.95 and 0.92, while MSD accuracy is 0.94 and 0.95, respectively. This supports the robustness of the model across various datasets for medical imaging analysis. The loss of training and testing is designed in Fig. 8 (a–c). The BraTS dataset has attained training and testing loss of 0.08 and 0.14. The FETS dataset has obtained losses of 0.1 and 0.17. The MSD dataset has obtained losses of 0.13 and 0.21. The overall epochs employed for training and testing are between 0 and 50. The x-axis is provided on the loss value and the y-axis is provided on the epoch.

The cross-validation performance of the model with three databases is specified in Fig. 9(a–c). For strengthening the proposed model, a k-fold cross-validation method is employed. The metrics utilized for the evaluation are precision, F1 score accuracy, sensitivity, and specificity. The BraTS 2019 dataset, the accuracy achieved in fold 1 and fold 10 ranging 95.2–98.9 %, precision from 93.5 % to 97.82 %, sensitivity from 94.8 % to 98.1 %, specificity from 93 % to 97.1 %, and F1 score from 94 % to 98.5 % across folds. Similarly, in the FETS dataset, performance is achieved with accuracy ranging from 94.3 % to 97.6 %, precision from 92.7 % to 96.75 %, sensitivity from 93.8 % to 97.13 %, specificity from 92 % to 96.05 %, and F1 score from 93 % to 97.45 %. Moreover, the MSD dataset, accuracy varying from 92.1 % to 96.1 %, precision from 90.1 % to 94.62 %, sensitivity from 90.5 % to 95.15 %, specificity from 89 % to 94.1 %, and F1 score from 91 % to 95.55 %. These results demonstrate the model's robustness across multiple

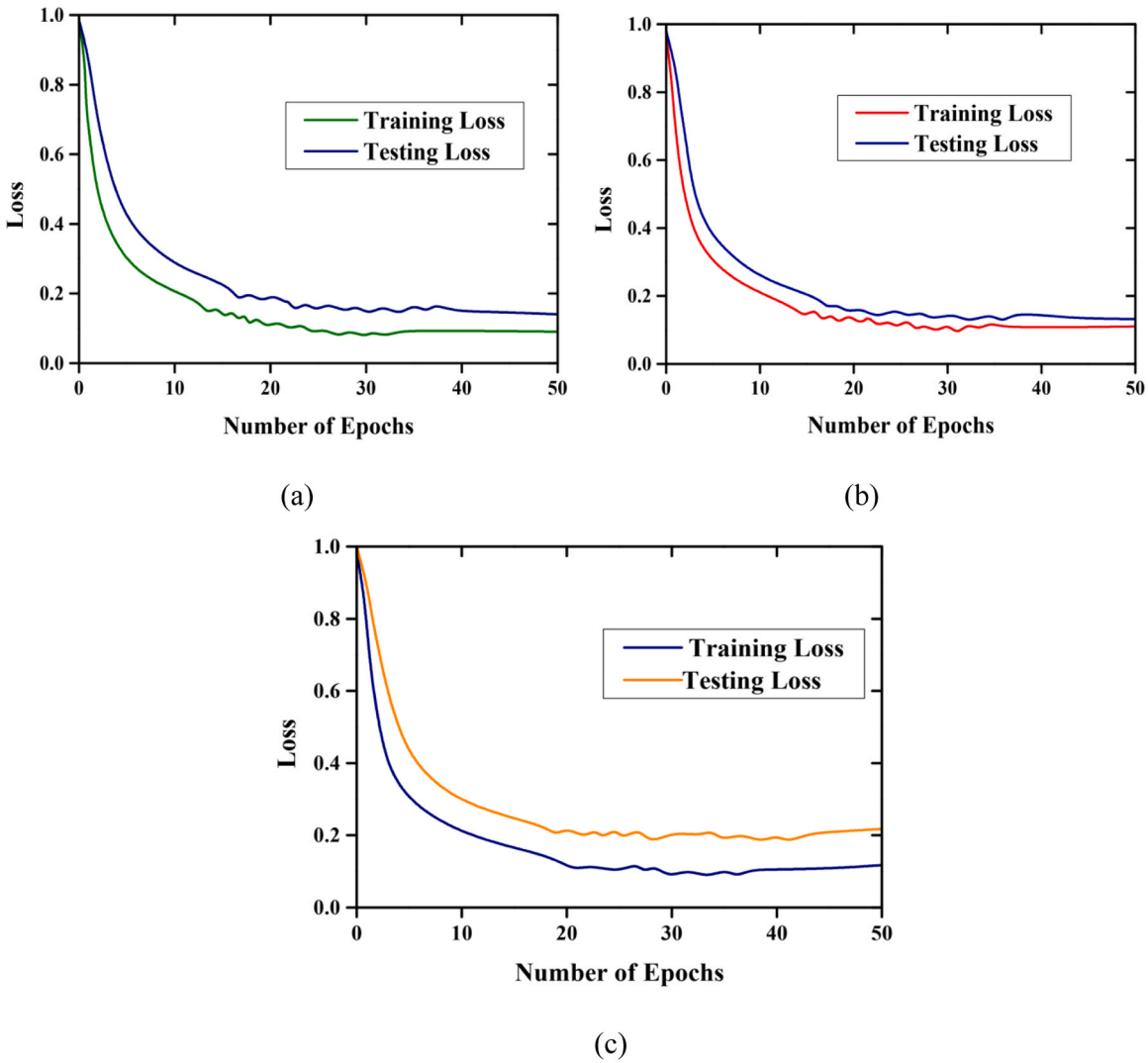

Fig. 8. Training and testing loss (a) BraTS 2019 dataset (b) FETS dataset (c) MSD dataset.

datasets, demonstrating its capability for accurate and robust medical imaging analysis and demonstrating its clinical applicability.

The proposed technique is contrast with several existing methods to verify the potency of model. The techniques used for the comparative analysis are DTNet [32], CNN [33], SVM [34], KNN-RF-DT [35], GBM [36], TD-CNN-LSTM [43] and ConvLSTM [44]. The comparative analysis of the BraTs 2019 dataset is provided in Fig. 10. The various methods are given on x-axis while the performance rate is given on y-axis. The suggested technique has attained an accuracy of 98.9 %, better precision of 97.82 %, sensitivity of 98.1 %, specificity of 97.1 %, and F1 score of 98.5 %. Based on our experimental results, it is obvious that brain tumor analysis is very rapid and accurate when compared to manual detection done by a radiologist or medical specialist.

Table 3 shows the execution time of various methods compared to our proposed method. Our proposed method achieved a low execution time (2.5 min) compared to existing methods such as DTNet, CNN, SVM, KNN-RF-DT, GBM, ConvLSTM, and TD-CNN-LSTM methods which have longer processing times. This efficiency demonstrates the efficiency and usability of our method, making it a preferred option for time-critical applications in the medical imaging analysis domain.

The ablation tests are conducted using the enhanced ConvLSTM for classifying based PCA and RFE module for feature selection and U-Net for Anomaly region segmentation. The results are presented in Table 4. Since the computational pressure factors are applied to the effectiveness of the models are measured by accuracy. However, computational pressure parameters also increased as a consequence of these approaches. Hence, our technique is more precise than the other techniques. This indicates that our technique did well in improving the method's ability to concentrate on important information whereas disregarding noise. The advantages of our technique to increase performance are presented in the ablation test results.

4.6. Discussion

The suggested method has shown better results in the classification of anomalies in the patient's 3D MRI scan. This model is highly useful for radiologists and medical professionals in the tracking and detection of brain cancer. It leads to earlier detection and improved patient outcomes. The proposed model is based on cross-validations like K-fold cross-validation. This indicates that the model performs well across various subsets of data. This validates the model's reliability in real-world situations. The suggested model performs better according to sensitivity, accuracy, sensitivity, specificity, F1 score, and simulation time when compared to the methods currently in use. Our approach to overcoming the difficulties of anomaly classification in MRI scans.

4.6.1. Limitation

Even though the proposed ConvLSTM model gains remarkable

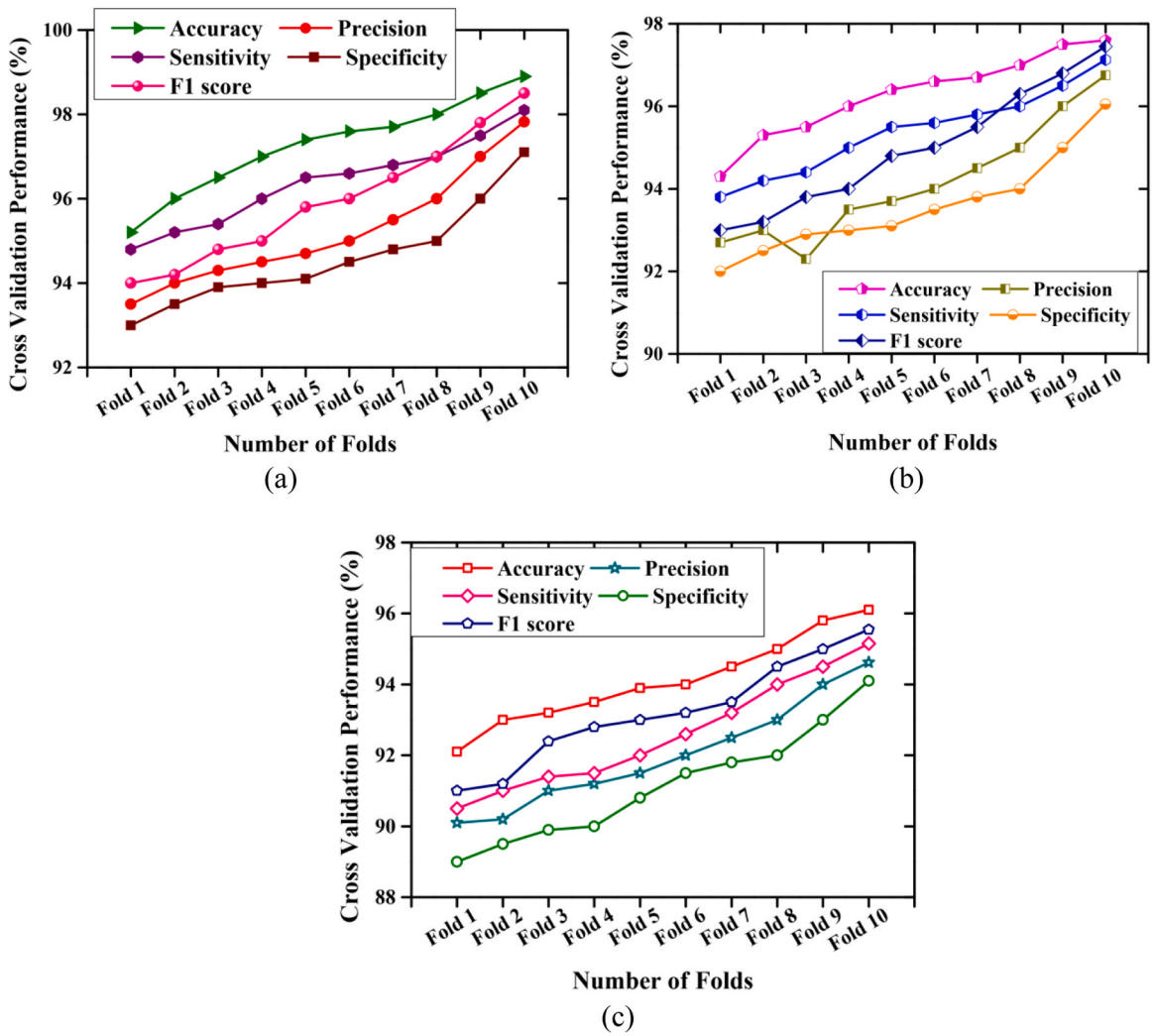

Fig. 9. Cross-validation performance (a) BraTS 2019 dataset (b) FETS dataset (c) MSD dataset.

detection efficiency in anomaly detection using 3D MRI scans, the limitation exists in terms of fine-tuning, scalability and data quality. In real-world application like clinical diagnosis, data quality is one of the crucial aspects of training. Even if we used resizing and normalization techniques, the quality enhancement techniques provide more reliable prediction results. This work lacks such image enhancement procedure; so as a future plan, we will incorporate the improvement approach for better accuracy. Another significant consideration is parameter optimization. Nowadays, many metaheuristic algorithms are developed to stand against challenges posed by complex optimization issues. The traditional optimizer like Adam might result in suboptimal performance, which in future be replaced by modern metaheuristic optimizer for fine-tuning process. In addition, scalability investigation to assess the model efficiency of handling high data volume is needed to be done.

5. Conclusion

In this study, we present robust and efficient methodology for the detection of anomaly regions within 3D MRI scan data. This method addresses critical challenges in the preprocessing of data, segmentation of data, feature extraction dimensionality reduction, and classification of data. The proposed approach uses DL techniques, including U-Net for segmentation and ConvLSTM for classification. The proposed approach demonstrates robustness and effectiveness in identifying anomaly regions within brain imaging data. By Incorporating statistical feature extraction techniques and dimensionality reduction methods such as PCA and RFE, this model optimizes the selection of discriminant features while reducing computational complexity. The ConvLSTM's architecture, which allows for the capture of spatial patterns, is a novel approach to MI analysis. This approach is especially suitable for dynamic anomaly detection in volume data, providing valuable insights for diagnostic and treatment planning. The proposed model has achieved an accuracy of 98.9 %, precision of 97.82 %, sensitivity of 98.1 %, specificity of 97.1 %, F1 score of 98.5 %, and execution time of 2.5 minutes. The proposed research holds significant promise for clinical applications. By enhancing the accuracy and speed of anomaly detection within 3D MRI scans, the diagnosis process is expedited, enabling healthcare professionals to make informed decisions swiftly. Early diagnosis is particularly crucial for patients with complex medical conditions like glioblastoma, where timely intervention significantly impacts outcomes. The presented methodology opens avenues for future study and advancement in the analysis of MI field:

- *Multi-Class Anomaly Detection*: Extending the model to classify and differentiate between various anomaly types within MRI scans, such as different tumor subtypes, can enhance diagnostic precision.
- *Transfer Learning (TL):* Researching the application of TL from pre-trained methods on larger database could further improve the model's performance, especially in cases with limited training data.

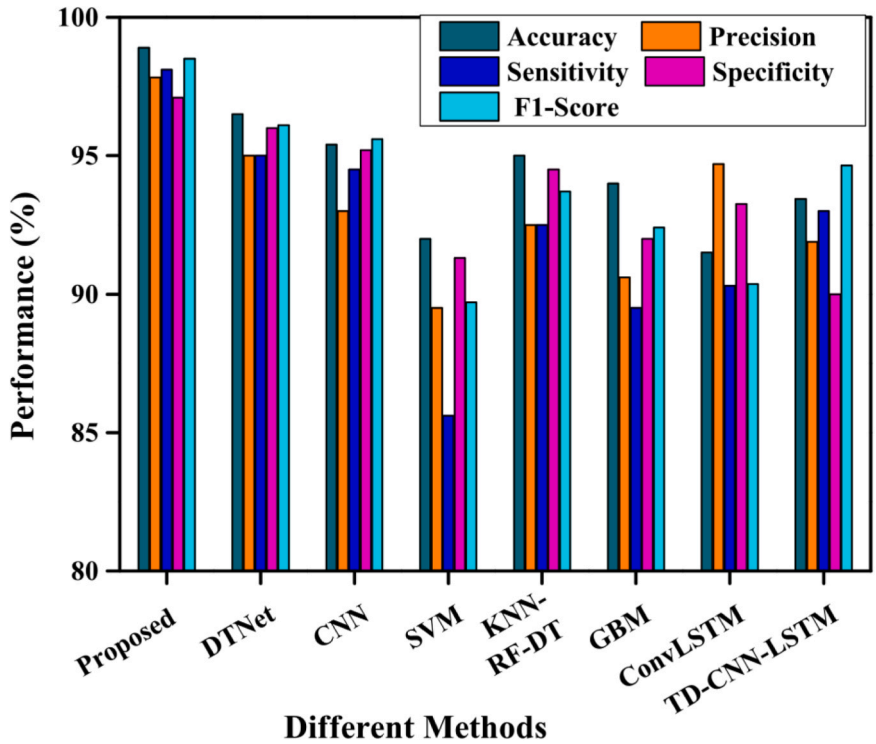

Fig. 10. Comparative analysis of proposed technique vs existing techniques.

Table 3
Comparison of simulation times of the proposed techniques vs existing techniques.

Different methods	Execution time (min)
DTNet	8
CNN	12
SVM	21
KNN-RF-DT	14
GBM	15
ConvLSTM	5.3
TD-CNN-LSTM	6.7
Proposed	2.5

Table 4
Ablation Study of our proposed method.

Methods				Accuracy (%)
Anomaly region segmentation	Feature selection		Classification	
U-Net	*PCA*	*RFE*	*ConvLSTM*	
✓	×	×	×	89.02
×	✓	✓	×	92.87
×	×	×	✓	90.98
✓	×	×	✓	94.85
✓	✓	✓	✓	98.9

- *Interpretable AI:* Developing methods to interpret the model's decisions and provide visual or textual explanations for anomaly detection can enhance trust and adoption by healthcare practitioners.

CRediT authorship contribution statement

Syed Shameem: Formal analysis, Investigation, Project administration. **M. Rajkumar:** Project administration, Resources. **E.S. Madhan:** Project administration, Software. **Anuradha Durairaj:** Investigation, Methodology.

Declaration of Competing Interest

The authors declare that they have no known competing financial interests or personal relationships that could have appeared to influence the work reported in this paper.

Data availability

Data will be made available on request.

References

[1] (a) J. van der Geer, J.A.J. Hanraads, R.A. Lupton, The art of writing a scientific article, J. Sci. Commun. 163 (2010) 51–59, https://doi.org/10.1016/j.Sc.2010.00372;
(b) D. Pradeep, M.K. Tembhre, A.S. Parihar, C. Rao, Magnetic resonance imaging: basic principles and advancement in clinical and diagnostics approaches in health care, in: Biomedical Imaging Instrumentation, Academic Press, 2022, pp. 45–66.
[2] W.H. Pinaya, P.D. Tudosiu, R. Gray, G. Rees, P. Nachev, S. Ourselin, M.J. Cardoso, Unsupervised brain imaging 3D anomaly detection and segmentation with transformers, Med. Image Anal. 79 (2022) 102475.
[3] K.M. van Hespen, J.J. Zwanenburg, J.W. Dankbaar, M.I. Geerlings, J. Hendrikse, H. J. Kuijf, An anomaly detection approach to identify chronic brain infarcts on MRI, Sci. Rep. 11 (1) (2021) 7714.
[4] T. Ghosh, M.I.A. Palash, M.A. Yousuf, M.A. Hamid, M.M. Monowar, M.O. Alassafi, A robust distributed deep learning approach to detect Alzheimer's disease from MRI images, Mathematics 11 (12) (2023) 2633.
[5] C. Han, L. Rundo, K. Murao, T. Noguchi, Y. Shimahara, Z.Á. Milacski, S. Koshino, E. Sala, H. Nakayama, S.I. Satoh, MADGAN: unsupervised medical anomaly detection GAN using multiple adjacent brain MRI slice reconstruction, BMC Bioinform. 22 (2) (2021) 1–20.
[6] M. Bahri, F. Salutari, A. Putina, M. Sozio, AutoML: state of the art with a focus on anomaly detection, challenges, and research directions, Int. J. Data Sci. Anal. 14 (2) (2022) 113–126.
[7] M. Bengs, F. Behrendt, J. Krüger, R. Opfer, A. Schlaefer, Three-dimensional deep learning with spatial erasing for unsupervised anomaly segmentation in brain MRI, Int. J. Comput. Assist. Radiol. Surg. 16 (2021) 1413–1423.
[8] K. Ramaraj, V. Govindaraj, Y.D. Zhang, P.R. Murugan, S.H. Wang, A. Thiyagarajan, S. Sankaran, Agnostic multimodal brain anomalies detection using a novel single-structured framework for better patient diagnosis and therapeutic planning in clinical oncology, Biomed. Signal Process. Control 77 (2022) 103786.

[9] L. Kang, Z. Zhou, J. Huang, W. Han, I.E.E.E. Member, Renal tumors segmentation in abdomen CT images using 3D-CNN and ConvLSTM, Biomed. Signal Process. Control 72 (2022) 103334.
[10] M. Ma, X. Zhang, Y. Li, X. Wang, R. Zhang, Y. Wang, P. Sun, X. Wang, X. Sun, ConvLSTM coordinated longitudinal transformer under spatio-temporal features for tumor growth prediction, Comput. Biol. Med. 164 (2023) 107313.
[11] N.S. Shaik, T.K. Cherukuri, Multi-level attention network: application to brain tumor classification, Signal Image Video Process. 16 (3) (2022) 817–824.
[12] L. Liu, P. Zhang, G. Liang, S. Xiong, J. Wang, G. Zheng, A spatiotemporal correlation deep learning network for brain penumbra disease, Neurocomputing 520 (2023) 274–283.
[13] G. Luo, W. Xie, R. Gao, T. Zheng, L. Chen, H. Sun, Unsupervised anomaly detection in brain MRI: learning abstract distribution from massive healthy brains, Comput. Biol. Med. 154 (2023) 106610.
[14] E. Özbay, F.A. Özbay, F.S. Gharehchopogh, Peripheral blood smear images classification for acute lymphoblastic leukemia diagnosis with an improved convolutional neural network, J. Bionic Eng. (2023) 1–17.
[15] M. Ayar, A. Isazadeh, F.S. Gharehchopogh, M. Seyedi, Chaotic-based divide-and-conquer feature selection method and its application in cardiac arrhythmia classification, J. Supercomput. (2022) 1–27.
[16] F.S. Gharehchopogh, S. Ghafouri, M. Namazi, B. Arasteh, Advances in Manta ray foraging optimization: a comprehensive survey, J. Bionic Eng. (2024) 1–38.
[17] F.S. Gharehchopogh, T. Ibrikci, An improved African vultures optimization algorithm using different fitness functions for multi-level thresholding image segmentation, Multimed. Tools Appl. 83 (6) (2024) 16929–16975.
[18] F.S. Gharehchopogh, B. Abdollahzadeh, S. Barshandeh, B. Arasteh, A multi-objective mutation-based dynamic Harris Hawks optimization for botnet detection in IoT, Internet Things 24 (2023) 100952.
[19] R. Ranjbarzadeh, A. Bagherian Kasgari, S. Jafarzadeh Ghoushchi, S. Anari, M. Naseri, M. Bendechache, Brain tumor segmentation based on deep learning and an attention mechanism using MRI multi-modalities brain images, Sci. Rep., vol. 11 (no. 1), p. 10930.
[20] N. Kakhandaki, S.B. Kulkarni, Classification of brain MR images based on bleed and calcification using ROI cropped U-Net segmentation and ensemble RNN classifier, Int. J. Inf. Technol. (2023) 1–16.
[21] R.Y. Lu, Y. Bagdasarova, A.Y. Lee, Machine learning–based anomaly detection techniques in ophthalmology, JAMA Ophthalmol. 140 (2) (2022) 189–190.
[22] N.F. Aurna, M.A. Yousuf, K.A. Taher, A.K.M. Azad, M.A. Moni, A classification of MRI brain tumor based on two stage feature level ensemble of deep CNN models, Comput. Biol. Med. 146 (2022) 105539.
[23] M.F. Alanazi, M.U. Ali, S.J. Hussain, A. Zafar, M. Mohatram, M. Irfan, R. AlRuwaili, M. Alruwaili, N.H. Ali, A.M. Albarrak, Brain tumor/mass classification framework using magnetic-resonance-imaging-based isolated and developed transfer deep-learning model, Sensors 22 (1) (2022) 372.
[24] S. Chatterjee, A. Sciarra, M. Dünnwald, P. Tummala, S.K. Agrawal, A. Jauhari, A. Kalra, S. Oeltze-Jafra, O. Speck, A. Nürnberger, StRegA: unsupervised anomaly detection in brain MRIs using a compact context-encoding variational autoencoder, Comput. Biol. Med. 149 (2022) 106093.
[25] A. Akter, N. Nosheen, S. Ahmed, M. Hossain, M.A. Yousuf, M.A.A. Almoyad, K. F. Hasan, M.A. Moni, Robust clinical applicable CNN and U-Net based algorithm for MRI classification and segmentation for brain tumor, Expert Syst. Appl. 238 (2024) 122347.
[26] N. Wang, C. Chen, Y. Xie, L. Ma, Brain tumor anomaly detection via latent regularized adversarial network, arXiv preprint arXiv:2007, 2020, p. 04734.
[27] J. Jin, H. Zhou, S. Sun, Z. Tian, H. Ren, J. Feng, X. Jiang, Machine learning based gray-level co-occurrence matrix early warning system enables accurate detection of colorectal cancer pelvic bone metastases on MRI, Front. Oncol. 13 (2023) 1121594.
[28] J. Amin, M. Sharif, M. Yasmin, S.L. Fernandes, A distinctive approach in brain tumor detection and classification using MRI, Pattern Recognit. Lett. 139 (2020) 118–127.
[29] B.A. Skourt, A. Majda, N.S. Nikolov, A. Begdouri, Multi-scale ConvLSTM attention-based brain tumor segmentation, Int. J. Adv. Comput. Sci. Appl., vol. 13(no. 11).
[30] K.K. Wong, W. Xu, M. Ayoub, Y.L. Fu, H. Xu, R. Shi, M. Zhang, F. Su, Z. Huang, W. Chen, Brain image segmentation of the corpus callosum by combining bi-directional convolutional LSTM and U-Net using multi-slice CT and MRI, Comput. Methods Prog. Biomed. 238 (2023) 107602.
[31] J.G. SivaSai, P.N. Srinivasu, M.N. Sindhuri, K. Rohitha, S. Deepika, An automated segmentation of brain MR image through fuzzy recurrent neural network, in: Bio-inspired Neurocomputing, 2020, pp. 163–179.
[32] A. Raza, H. Ayub, J.A. Khan, I. Ahmad, S.A. Salama, Y.I. Daradkeh, D. Javeed, A. Ur Rehman, H. Hamam, A hybrid deep learning-based approach for brain tumor classification, Electronics 11 (7) (2022) 1146.
[33] T. Tazin, S. Sarker, P. Gupta, F.I. Ayaz, S. Islam, M. Monirujjaman Khan, S. Bourouis, S.A. Idris, H. Alshazly, A robust and novel approach for brain tumor classification using convolutional neural network, Comput. Intell. Neurosci. (2021).
[34] C.S. Rao, K. Karunakara, Efficient detection and classification of brain tumor using kernel based SVM for MRI, Multimed. Tools Appl. 81 (5) (2022) 7393–7417.
[35] G. Garg, R. Garg, Brain tumor detection and classification based on hybrid ensemble classifier, arXiv preprint arXiv:2101.00216, 2021.
[36] N. Chintalapudi, G. Battineni, L.M. Goyal, F. Amenta, Brain tumor classifications by gradient and XG boosting machine learning models, in: Predictive Modeling in Biomedical Data Mining and Analysis, Academic Press, 2022, pp. 123–136.
[37] S. Bakas, M. Reyes, A. Jakab, S. Bauer, M. Rempfler, A. Crimi, R.T. Shinohara, C. Berger, S.M. Ha, M. Rozycki, M. Prastawa, Identifying the best machine learning algorithms for brain tumor segmentation, progression assessment, and overall survival prediction in the BRATS challenge, arXiv preprint arXiv:1811.02629, 2018.
[38] S. Bakas, H. Akbari, A. Sotiras, M. Bilello, M. Rozycki, J.S. Kirby, J.B. Freymann, K. Farahani, C. Davatzikos, Advancing the cancer genome atlas glioma MRI collections with expert segmentation labels and radiomic features, Sci. Data 4 (1) (2017) 1–13.
[39] B.H. Menze, A. Jakab, S. Bauer, J. Kalpathy-Cramer, K. Farahani, J. Kirby, Y. Burren, N. Porz, J. Slotboom, R. Wiest, L. Lanczi, The multimodal brain tumor image segmentation benchmark (BRATS), IEEE Trans. Med. Imaging 34 (10) (2014) 1993–2024.
[40] S. Pati, U. Baid, M. Zenk, B. Edwards, M. Sheller, G.A. Reina, P. Foley, A. Gruzdev, J. Martin, S. Albarqouni, Y. Chen, The federated tumor segmentation (fets) challenge, arXiv preprint arXiv:2105.05874, 2021.
[41] A.L. Simpson, M. Antonelli, S. Bakas, M. Bilello, K. Farahani, B. Van Ginneken, A. Kopp-Schneider, B.A. Landman, G. Litjens, B. Menze, O. Ronneberger, A large annotated medical image dataset for the development and evaluation of segmentation algorithms, arXiv preprint arXiv:1902.09063, 2019.
[42] M. Antonelli, A. Reinke, S. Bakas, K. Farahani, A. Kopp-Schneider, B.A. Landman, G. Litjens, B. Menze, O. Ronneberger, R.M. Summers, B. Van Ginneken, The medical segmentation decathlon, Nat. Commun. 13 (1) (2022) 4128.
[43] S. Montaha, S. Azam, A.R.H. Rafid, M.Z. Hasan, A. Karim, A. Islam, Timedistributed-cnn-lstm: a hybrid approach combining cnn and lstm to classify brain tumor on 3d mri scans performing ablation study, IEEE Access 10 (2022) 60039–60059.
[44] K.S. Raju, S. Arvind, R. Chegoni, V.A. Naryana, A. Vivekananda, C.R.K. Babu, Assessment of 3D MRI image segmentation and classification for brain tumor detection using ConvLSTM, in: Proceedings of the 2023 IEEE 5th International Conference on Cybernetics, Cognition and Machine Learning Applications (ICCCMLA), IEEE, 2023, October, pp. 665–70.